

Article

Off-Design Performances of Subcritical and Supercritical Organic Rankine Cycles in Geothermal Power Systems under an Optimal Control Strategy

Tieyu Gao * and Changwei Liu

Institute of Turbomachinery, School of Energy and Power Engineering, Xi'an Jiaotong University, Xi'an 710049, China; c.1985.02.05@stu.xjtu.edu.cn

* Correspondence: sunmoon@mail.xjtu.edu.cn; Tel.: +86-13201896087

Received: 19 July 2017; Accepted: 9 August 2017; Published: 11 August 2017

Abstract: The conditions of heat source and heat sink in a geothermal ORC system may frequently vary due to variations in geological conditions, ambient temperature and actual operation. In this study, an off-design performance prediction model for geothermal ORC systems is developed according to special designs of critical components, and an optimal control strategy which regards the turbine guide vane angle, the refrigerant pump rotational speed and the cooling water mass flow rate as control variables is proposed to maximize the net power output. Off-design performances of both subcritical and supercritical ORCs are analyzed. The results indicate that, under the optimal control strategy, the net power output of both ORCs increase with greater geothermal water mass flow rate, higher geothermal water inlet temperature and lower cooling water inlet temperature, which is mainly due to a greater working fluid mass flow rate, higher turbine inlet pressure and lower condensing pressure, respectively. The net power output of supercritical ORC is always greater than that of subcritical ORC within the range of this study, but the difference tends to decrease when supercritical ORC activates the geothermal water reinjection temperature restriction.

Keywords: Organic Rankine Cycle; geothermal power system; off-design performance; control strategy

1. Introduction

Due to the rapid growth of the world economy, the global energy consumption continues to increase significantly, which leads to excessive consumption of fossil fuels and serious environmental deterioration. In this instance, the utilization of low-grade thermal energy, including geothermal energy, solar energy, biomass energy and industrial waste heat, is currently drawing great attention. Geothermal energy presents favorable application prospects owing to its abundant storage capacity and convenient utilization. Among all the available technologies, the Organic Rankine Cycle (ORC) has been regarded as an efficient approach to convert low-grade heat into electricity. A great amount of research concentrated on working fluid selection and system design has been conducted to enhance the performance of ORC systems. Chen et al. [1] screened 35 kinds of working fluids for the subcritical and supercritical ORCs and proposed the selection criteria of working fluids. Zhang et al. [2] compared various working fluids for a low temperature ORC system with five different indicators as criteria. Both subcritical and supercritical ORCs were examined, and it turned out that supercritical ORC using R125 had good economics and high geothermal utilization rates. Guo et al. [3] reported that the choice of optimal working fluid was determined by the profiles of the heat source and heat sink, and the introduction of a regenerator did not always enhance the system efficiency. Liu et al. [4] pointed out that supercritical ORC could yield good performances in both thermodynamic and economic aspects, and R134a was the optimal working fluid.

These previous ORC studies were mainly focused on design conditions, however, the heat source and sink conditions probably vary during the actual operation of an ORC, which makes the operating condition deviate from the design point. Consequently, the off-design performance of ORC is of great importance and should be carefully investigated. The critical components of an ORC system, mainly including the expander and heat exchangers, significantly influence the system performance. For expanders, many studies have been carried out on the radial inflow turbine which is regarded as a suitable candidate for ORC. Sauret and Rowlands [5] preliminarily designed radial inflow turbines for a geothermal ORC system with five different working fluids, and discovered that the turbines had similar efficiencies but great distinctions in dimensions. Pan and Wang [6] pointed out the disadvantage of a given isentropic efficiency of a turbine in ORC analysis, then they computed the optimal internal efficiency of radial inflow turbines under different conditions to improve the reliability of the analysis. Baines [7] revised the loss models and proposed a mean-line model of radial inflow turbine based on NASA studies. The model could predict the turbine performance under various conditions, and the dependability of this model had been verified by a database of turbine experiments. Li and Ren [8] designed a radial inflow turbine using R123 based on one-dimensional method and performed numerical simulation of the designed turbine. The numerical results agreed well with the designed values, indicating that the one-dimensional method was reliable. Zheng et al. [9] presented a full design process of a radial inflow turbine used in ORC. Both one-dimensional calculation and three-dimensional Computational Fluid Dynamics (CFD) simulations were conducted, and the results showed a good agreement. Then off-design performance analysis was performed with the one-dimensional method which was considered to be convenient and accurate. For heat exchangers, Wang et al. [10] employed the log mean temperature difference method to compute the heat transfer area of plate type condenser and conducted a multi-objective optimization to obtain the optimal condenser geometry design. Calise et al. [11] investigated the influences of geometry parameters of heat exchangers on ORC performance and found that evaporator displayed a very different trend. Song et al. [12] established a prediction model of heat exchangers according to the efficiency-NTU (number of transfer unit) method, then the model was applied to analyze the off-design performance of ORC.

Generally, under off-design conditions, a specific control strategy ought to be adopted to maintain the steady operation of an ORC system. In view of the thermal degradation of geothermal resources, Gabbrielli [13] developed a detailed supercritical ORC off-design performance model to determine the optimal design parameters. The expander operated in sliding pressure mode with constant nozzle area to satisfy various operation conditions. It turned out that the ORC system designed based on the lowest geothermal temperature displayed the best economic performance. Fu et al. [14,15] conducted off-design performance analysis of a 250-kW ORC system with variable heat source temperatures and flow rates. A pressure control method was applied to ensure R245fa was in liquid and vapor saturation states at the exits of the preheater and evaporator, respectively. It turned out that higher temperature and greater flow rate of heat source led to increases in both net power output and thermal efficiency. Nevertheless, they only considered the off-design performance of the preheater. Ibarra et al. [16] researched the off-design performance of ORCs from a thermodynamic perspective and discovered that the isentropic efficiency of a scroll expander significantly influenced the cycle performance. In this work, both expander rotation speed and working pressure were regulated to satisfy different load demands. Nusiaputra et al. [17] focused on the thermal-economic performance of ORCs utilized in a mid-enthalpy geothermal power system. In order to obtain optimal operating points under off-design conditions, evaporation pressure, turbine inlet temperature and condensation temperature were respectively controlled by the turbine nozzle opening, pump speed and fan speed. Mazzi et al. [18] established a comprehensive dynamic model of a regenerative ORC to explore the influences of heat source flow rate and heat sink temperature on the cycle performance. Three PID (Proportion Integration Differentiation) controllers were employed to keep the system stable and meet actual operating constraints under off-design conditions. To develop a more accurate and reliable off-design analysis method of ORC, Hu et al. [19,20] specially designed the critical components including radial inflow turbine and plate heat exchangers for a subcritical ORC.

Under different heat sources conditions, sliding pressure operation, constant pressure operation, and an optimal control strategy combining the former two methods were studied, respectively. The results showed that the optimal control strategy was superior to the other two methods. However, the variation of heat sink condition was not considered in their works. Usman et al. [21] compared the part-load operation of air cooled and cooling water tower-based geothermal ORC systems installed at different geographical locations. A sink auxiliary control optimization was performed to provide maximum power output at off-design conditions by changing the fan speed of cooling tower, air cooled condenser and mass flow rate of sink side. Rajabloo et al. [22] investigated the behaviors of low temperature and high temperature ORCs with varying conditions of the heat source and heat sink, respectively. The turbine inlet pressure, the condensing pressure and the mass flow rate of working fluid following were regulated to meet cycle requirements at off-design conditions. They considered the thermal decomposition of the working fluid and found that the properties of decomposed products could significantly affect cycle efficiency. To study the off-design performance of a small scale subcritical ORC, Liu et al. [23] developed a working fluid charge oriented model based on the component models and discovered that the optimal working fluid charge volume would differ depending on the expander's output work. In this study, the solution of off-design model was based on the optimization of pump rotation speed to keep the system output to a stable value.

Most investigations focused on the off-design analysis of ORC were conducted based on the performance curves or simple formulas of critical components which were not specially obtained from ORC systems. Hence, predicting the off-design performance on the basis of specially designed components would be more dependable. In addition, few studies have compared the off-design performances of subcritical and supercritical ORCs with a specific control strategy. In this paper, to analyze and compare off-design performances of subcritical and supercritical geothermal ORCs with a water cooling system, an off-design performance prediction model is developed based on special designs of the critical components. Then a specific optimal control strategy which maximizes the net power output is proposed to regulate the operating parameters of both ORCs with varying geothermal water mass flow rate, geothermal water temperature and cooling water temperature. The control variables of the control strategy are turbine guide vane angle, rotational speed of refrigerant pump and cooling water mass flow rate. The findings can provide references and guidelines for the off-design operation regulation of a geothermal ORC system.

2. ORC System

In this work, both subcritical and supercritical ORCs are adopted to utilize the geothermal energy. The layout of geothermal ORC system and T-S diagrams are displayed in Figures 1 and 2, respectively. The following processes are included in ORC:

- 1–2: The high pressure working fluid vapor expands to do work in the turbine.
- 2–5: The exhausted vapor is condensed by cooling water in the condenser.
- 5–6: The subcooled liquid is pumped to a high pressure in the refrigerant pump.
- 6–1: The high pressure liquid is heated into vapor by geothermal water in the evaporator (vapor generator).

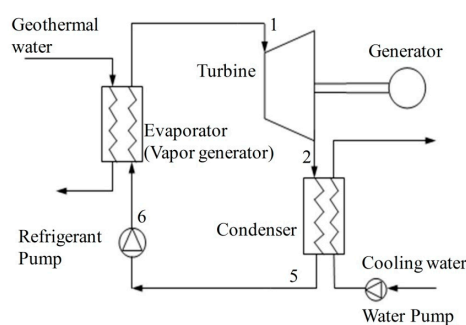


Figure 1. The layout of a geothermal ORC system.

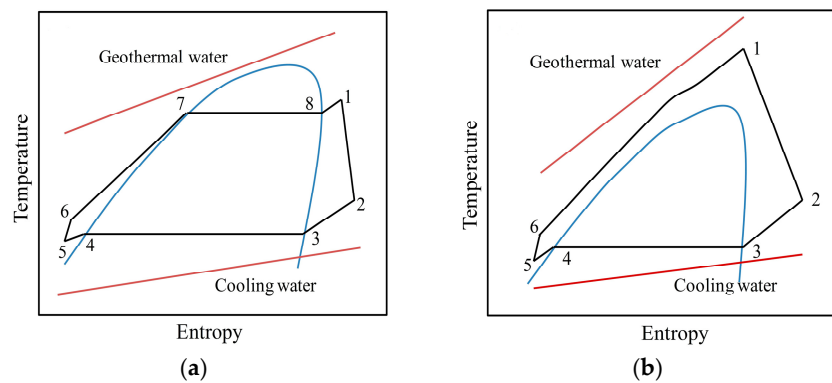


Figure 2. T-S diagram: (a) Subcritical ORC; and (b) Supercritical ORC.

2.1. Thermodynamic Modeling

The power yielded by turbine, consumed by the refrigerant pump and cooling water pump are respectively expressed as:

$$P_{Turbine} = m_{wf}(h_1 - h_{2,s})\eta_{Turbine} = m_{wf}(h_1 - h_2) \quad (1)$$

$$P_{RP} = \frac{m_{wf}(h_{6,s} - h_5)}{\eta_{RP}} = m_{wf}(h_6 - h_5) \quad (2)$$

$$P_{WP} = \frac{m_{cw}gH}{\eta_{WP}} \quad (3)$$

Then the net power output of ORC is calculated as:

$$P_{net} = P_{Turbine} - P_{RP} - P_{WP} \quad (4)$$

2.2. Thermodynamic Parameter Optimization on the Design Condition

The design condition of the geothermal system is given as Table 1. For subcritical ORC, R600a is selected as a preferred working fluid [17,24,25]. Superheating is not advantageous for R600a which is a dry working fluid [26,27], so just a small superheating of 5 K is set to satisfy the practical operational constraints. For supercritical ORC, R134a is chosen due to its good performance [4,25]. To avoid cavitation in the refrigerant pump, a subcooling of 2 K is adopted in both ORCs. The regenerator cannot always enhance the thermodynamic performance of ORC at the expense of higher cost [25,27]. In addition, the regenerator can bring operative problems when geothermal water temperature is low under off-design conditions [13]. Therefore, the regenerator is not considered in this work. The geothermal water reinjection temperature should be not less than 70 °C to avoid silica oversaturation.

Table 1. Design operating conditions of the geothermal ORC system.

Parameter	Value
Geothermal water inlet temperature (°C)	150
Geothermal water reinjection temperature (°C)	≥70
Geothermal water flow rate (kg/s)	10
Cooling water inlet temperature (°C)	20
Evaporator pinch temperature (°C)	10
Vapor generator pinch temperature (°C)	10
Condenser pinch temperature (°C)	5
Turbine isentropic efficiency (%)	80
Refrigerant pump isentropic efficiency (%)	70
Cooling water pump head (m)	20
Cooling water pump efficiency (%)	80

To validate the models developed for the simulation of ORCs, the available data with the same operating conditions and working fluids in the literature are utilized. The comparisons of simulation results with those reported in literature are presented in Figure 3. As can be seen, there is a good agreement between the values of parameters calculated in this paper and those published in literature [24,28].

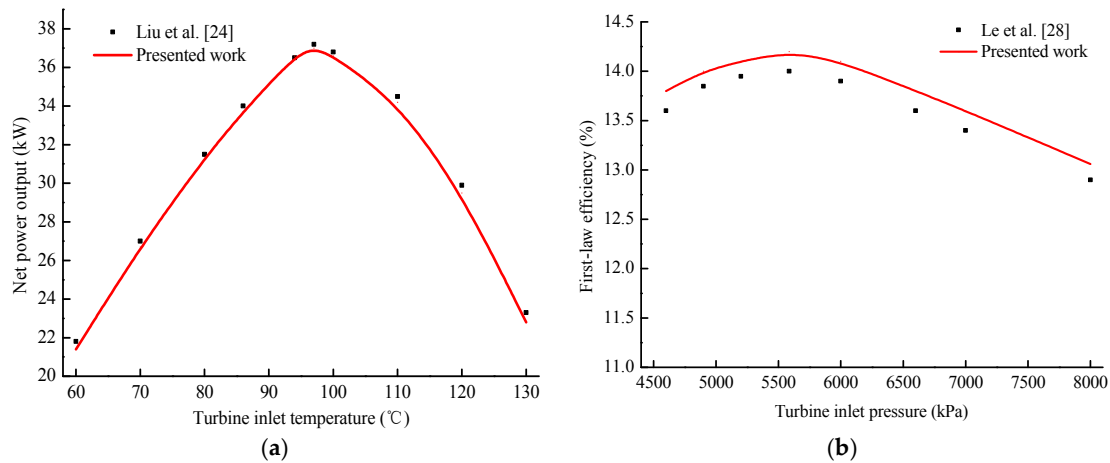


Figure 3. Model Validation: (a) Subcritical ORC; and (b) Supercritical ORC.

To conduct the thermodynamic performance calculation, some other thermodynamic variables need to be determined in addition to the parameters listed in Table 1. For subcritical ORC, the variables are turbine inlet pressure and condensation pressure, while for supercritical ORC, an additional variable, turbine inlet temperature should be considered. These variables are regarded as decision variables to conduct a single-objective optimization based on a genetic algorithm (GA). The net power output is chosen as optimization objective since the maximum value is desirable for a geothermal power system [29,30]. In this work, all the programs are written in MATLAB 2011b (The MathWorks, Natick, Massachusetts, USA), and the thermodynamic properties are attained from REFPROP 9.0 (NIST, Gaithersburg, Maryland, USA). Assumptions and constraints adopted are listed as below:

- (1) The system is supposed in steady state.
- (2) The pressure drops in heat exchangers and pipelines are ignored.
- (3) The vapor quality of turbine outlet is restricted to not less than 1 to avoid the droplet wear phenomenon.

The optimization results are displayed in Table 2. The specific internal parameters of ORCs can be calculated based on the optimal decision variable values, including the mass flow rates of working fluid and cooling water, inlet and outlet thermodynamic states of each component. Then the critical components can be specially designed.

Table 2. Optimization results of ORC systems on the design condition.

Parameter	Subcritical ORC	Supercritical ORC
Turbine inlet pressure (kPa)	1787.1	5106.6
Condensing pressure (kPa)	400.7	769.7
Turbine inlet temperature (°C)	99.4	132.8
Net power output (kW)	330.4	371.2
Mass flow rate of working fluid (kg/s)	8.07	15.06
Mass flow rate of cooling water (kg/s)	136.6	127.5

3. System Components Modeling and Design

To conduct the off-design performance analysis of ORC system, the performance prediction model and specific design of each important component should be determined.

3.1. Radial Inflow Turbine

Radial inflow turbines are characterized by easy manufacture, compact structures and high efficiency, and they are suitable for low flow rate and high pressure ratio situations. A variable inlet guide vane (VIGV) is a familiar method to adjust the radial turbine performance. The adjustable nozzles can rotate around the rotation centers, leading to the changes in nozzle outlet angle and area. Then the turbine performance can be regulated to adapt variable working conditions without throttling losses [31]. Thus, radial turbine with VIGV presents smooth off-design performance, and it is applied in this paper. A schematic of a radial inflow turbine is displayed in Figure 4.

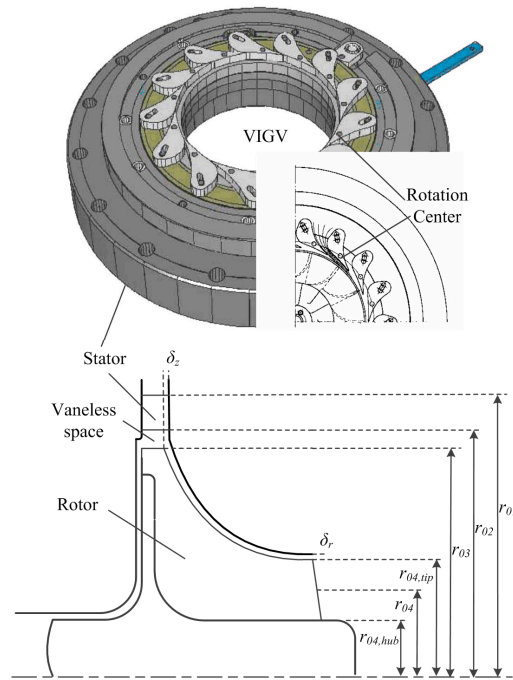


Figure 4. The schematic of radial inflow turbine.

The one-dimensional analysis method based on mass and energy conservation equations is employed to calculate the turbine performance. Compared with the computational fluid dynamics (CFD), this method is more convenient and practical, moreover, the prediction results can match well those of CFD [8,9]. In the turbine, the expansion process is preliminarily assumed to be isentropic, then relevant loss models are introduced to modify the flow process, making the prediction more accurate.

In stator vanes, the flow process can be expressed by the following equations:

$$h_{01} + \frac{c_{01}^2}{2} = h_{02} + \frac{c_{02}^2}{2} \quad (5)$$

$$m_{02} = \rho_{02} \cdot c_{02} \cdot \sin \alpha_{02} \cdot A_{out, stator} \quad (6)$$

Supersonic flow is common at the stator outlet in ORC, which leads to a critical flow rate. In such case, the stator outlet flow angle will deviate from the installation angle and should be corrected:

$$m_{02} = m_{cr} = \rho_{cr,02} \cdot c_{cr,02} \cdot A_{min, stator} \quad (7)$$

$$\sin \alpha_{02, correct} = \frac{m_{cr}}{\rho_{02} \cdot c_{02} \cdot A_{out, stator}} \quad (8)$$

A small clearance is set between the stator and rotor to avoid collision, and the tangential momentum is supposed to be conserved [32]:

$$c_{02,u} \cdot r_{02} = c_{03,u} \cdot r_{03} \quad (9)$$

$$m_{03} = \rho_{03} \cdot c_{03,r} \cdot A_{in,rotor} \quad (10)$$

In the rotors, the flow process can be expressed by:

$$h_{03} + \frac{w_{03}^2}{2} - \frac{u_{03}^2}{2} = h_{04} + \frac{w_{04}^2}{2} - \frac{u_{04}^2}{2} \quad (11)$$

$$m_{04} = \rho_{04} \cdot c_{04,r} \cdot A_{out,rotor} \quad (12)$$

Losses models which include stator loss (L_{stator}), incidence loss (L_i), passage loss (L_p), disc friction loss (L_{df}), clearance loss (L_c) and exit loss (L_e) are introduced in this work [33,34]:

$$L_{stator} = h_{02} - h_{02,s} = \frac{c_{02,s}^2(1 - K_{stator}^2)}{2} \quad (13)$$

$$L_i = \frac{w_{03}^2 \sin^2 n}{2} \quad (14)$$

$$L_p = K_p \left(\frac{w_{03}^2 \cos^2 n + w_{04}^2}{2} \right) \quad (15)$$

$$L_{df} = \frac{0.02125 \rho_{03} u_{03}^2 r_{03}^2}{m(\rho_{03} u_{03} r_{03} / \mu)^{0.2}} \quad (16)$$

$$L_c = \frac{u_{03}^3 Z_{rotor}}{8\pi} (K_z \delta_z M_z + K_r \delta_r M_r + K_{zr} \sqrt{\delta_z \delta_r M_z M_r}) \quad (17)$$

$$L_e = \frac{c_{04}^2}{2} \quad (18)$$

Then the turbine efficiency is given as:

$$\eta_{Turbine} = \frac{h_{01} - h_{04}^{st}}{h_{01} - h_{04,s}} \quad (19)$$

Based on the above equations, a turbine submodel is established to calculate the turbine performance on different operating conditions. By inputting geometric dimensions, rotational speed, backpressure and inlet thermodynamic parameters of the turbine, the efficiency and mass flow rate can be predicted through an iteration process. Here the pressures at stator outlet and rotor inlet are previously assumed, then the thermodynamic parameters and mass flow rate of each section of the turbine can be obtained. The iteration continues by adjusting the pressures until the mass flow rate of each section becomes equivalent, then the turbine performance can be acquired.

To verify the validity of the turbine submodel, the prediction result has been compared with the data from Hu et al. [19]. As displayed in Table 3, the submodel can predict the turbine performance within an acceptable error range. Subsequently, the turbines of subcritical and supercritical ORCs are specially designed based on the optimal thermodynamic parameters for the design conditions. A radial turbine design program was developed based on the method presented by Hu et al. [19]. In this program, the inlet pressure and temperature, mass flow rate and outlet pressure of the turbine listed in Table 2 are taken as input variables, and α_{02} , β_{02} , β_{04} , N , U/C_0 and r_{04}/r_{03} are selected as decision variables to regulate the geometric dimensions and turbine performance. In addition, structure restrictions are considered to guarantee the rationality of design. The efficiency of designed turbines should be close to 80%, which is the setting value in the thermodynamic parameter optimization on design condition. Satisfactory designs of turbines are obtained by adjusting the decision variables, and the design results are displayed in Table 4.

Table 3. Turbine submodel validation.

Parameter	Reference Data	Prediction Result	Deviation
Turbine efficiency (%)	82.3	82.7	0.5%
Mass flow rate (kg/s)	5.85	5.74	1.9%
Turbine outlet temperature (°C)	47.3	46.9	0.9%
Power (kW)	68.5	67.5	1.5%

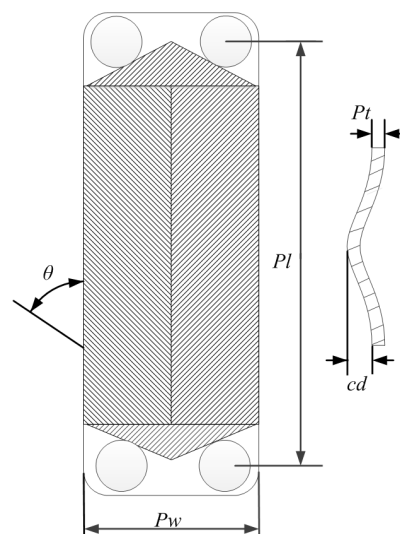
Table 4. Radial inflow turbines design results.

Parameter	Subcritical Turbine	Supercritical Turbine
r_{01} (mm)	159.8	119.3
r_{02} (mm)	135.8	101.4
r_{03} (mm)	123.5	92.2
$r_{04,tip}$ (mm)	85.8	52.7
$r_{04,hub}$ (mm)	60.2	25.8
b_{stator} (mm)	5.9	4.1
$b_{in,rotor}$ (mm)	5.9	4.1
α_{02} (°)	19	17
β_{04} (°)	29	36
Z_{stator} (mm)	14	14
Z_{rotor} (mm)	11	11
N (rpm)	17000	19000
$P_{Turbine}$ (kW)	402.9	498
$\eta_{Turbine}$ (%)	80.1	79.9

3.2. Heat Exchangers

Plate heat exchanger (PHE) has been increasingly used in various industries owing to its high heat transfer coefficient, simple maintenance, compact structure and less fouling. Queensland Geothermal Energy Centre of Excellence (QGECE) has been considering PHE as a favorite candidate for use in geothermal power systems [35]. A welded construction PHE without any gaskets which can work under temperatures beyond 400 °C and pressures up to 100 bar has been proposed for high temperature and pressure conditions [36], which means that welded construction PHEs can be used as vapor generators in supercritical ORCs.

In this study, PHEs are selected as evaporator (vapor generator) and condenser in both subcritical and supercritical ORCs. Chevron-type corrugation plates are adopted and the basic configuration of the PHE is displayed in Figure 5.

**Figure 5.** Basic configuration of the PHE.

The heat transfer process in each heat changer is divided into many small sections, and log mean temperature difference method is employed to calculate the heat transfer rate in each section:

$$Q = UA\Delta T_m \quad (20)$$

The pressure drop in heat exchanger is given by:

$$\Delta P = \frac{2fG^2}{\rho} \cdot \frac{Pl}{D} \quad (21)$$

For single-phase flow in evaporator and condenser, the Nusselt number and friction factor are given by Equations (22) and (23) [37,38].

$$Nu = 0.724 \left(\frac{6\theta}{\pi} \right)^{0.646} Re^{0.583} Pr^{1/3} \quad (22)$$

$$f = 2.99 / Re^{0.183} \quad (23)$$

A correlation obtained by experimental analysis is employed to calculate the heat transfer of supercritical fluid in vapor generator [35]:

$$Nu = 0.187 Re^{0.71} Pr^{0.35} \left(\frac{\tilde{c}_p}{c_{p,b}} \right)^{0.5} \left(\frac{\rho_w}{\rho_b} \right)^{0.3} \quad (24)$$

For the evaporation process in evaporator, the following correlations are adopted to determine the pressure drop and heat transfer, and θ_{\max} equals to 70° [39].

$$f = 15.698 C \left(\frac{G^2 D}{\rho_m \sigma} \right)^{-0.475} \left(\frac{\rho_l}{\rho_g} \right)^{-0.571} Bo^{0.255} \quad (25)$$

If $Bd < 4$

$$Nu = 982 \left(\frac{\theta}{\theta_{\max}} \right)^{1.101} \left(\frac{G^2 D}{\rho_m \sigma} \right)^{0.315} \left(\frac{\rho_l}{\rho_g} \right)^{-0.224} Bo^{0.320} \quad (26)$$

If $Bd \geq 4$

$$Nu = 18.495 \left(\frac{\theta}{\theta_{\max}} \right)^{0.248} \left(\frac{xGD}{\mu_g} \right)^{0.135} \left(\frac{GD}{\mu_l} \right)^{0.351} \left(\frac{\rho_l}{\rho_g} \right)^{0.223} Bo^{0.198} Bd^{0.235} \quad (27)$$

where:

$$Bd = \frac{(\rho_l - \rho_g)gD^2}{\sigma} \quad (28)$$

$$Bo = \frac{q}{G\gamma} \quad (29)$$

$$C = 2.125 \left(\frac{\theta}{\theta_{\max}} \right)^{9.993} + 0.955 \quad (30)$$

For condensation process in condenser, the Nusselt number and friction factor are respectively expressed as [40]:

$$Nu = 4.118 Re_{eq}^{0.4} Pr_l^{1/3} \quad (31)$$

$$f = 94.75 \left(\frac{p_m}{P_{cr}} \right)^{0.8} Bo^{0.5} Re^{-0.4} Re_{eq}^{-0.4} \quad (32)$$

in which P_{cr} denotes critical pressure, and equivalent Reynolds number is given as:

$$Re_{eq} = \frac{G_{eq}D}{\mu_l} \quad (33)$$

where:

$$G_{eq} = G \left[(1 - x) + x \left(\frac{\rho_l}{\rho_g} \right)^{0.5} \right] \quad (34)$$

If the geometric dimensions of a PHE are specified, the required heat transfer area can be calculated by above corresponding correlations, mass flow rates and thermodynamic parameters on both sides of the PHE. Under off-design conditions, the thermodynamic parameters at the ends of PHE and mass flow rates are not all known, and the required heat transfer area can be acquired by assuming the unknown quantities. The assumed quantities should be adjusted until the obtained area is consistent with the actual heat transfer area of PHE [20].

Afterwards the specific designs of evaporator (vapor generator) and condenser are performed in accordance to the optimal thermodynamic parameters on the design condition. All the PHEs are arranged as counterflow single-pass flow [10,19], and the pressure drops are limited to 2%. The design results of PHEs are displayed in Table 5.

Table 5. Heat exchangers design results.

Parameter	Evaporator (Subcritical ORC)	Condenser (Subcritical ORC)	Vapor Generator (Supercritical ORC)	Condenser (Supercritical ORC)
Plate width (m)	0.46	0.87	0.75	0.67
Plate length (m)	0.7	1.3	1.5	1.38
Plate thickness (mm)	0.6	0.6	0.6	0.6
Channel distance (mm)	3.0	3.1	2.5	3.1
Chevron angle (°)	60	60	60	60
Heat transfer area (m ²)	48.0	168.5	120.4	182.2
Pressure drop (kPa)	16.9	8.4	21.1	7.9

3.3. Pump

The methodology of the pump adopted in [16,19] is employed in this work. The non-dimensional performance curve of the refrigerant pump is derived from a centrifugal pump in a real power plant, as presented in Figure 6. The nominal rotational speed is assumed as 1500 rpm, and the efficiency comes to the maximum value of 70% at the design flow rate and head. For off-design conditions, the rotational speed can be adjusted, and the off-design performance can be acquired base on the non-dimensional performance curve and affinity laws.

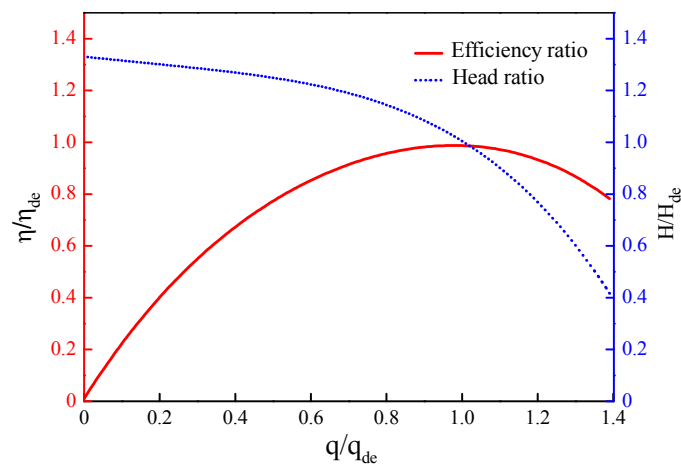


Figure 6. Performance curve of the refrigerant pump.

The cooling water pump makes cooling water flow circulate between condenser and cooling tower, and the power consumed by it is quite small. For simplicity, the head and efficiency of cooling water pump are taken as constant values displayed in Table 1 for off-design conditions.

4. Results and Discussion

4.1. Off-Design Performance Optimization

In a geothermal ORC system, the heat source and heat sink conditions may frequently vary due to the variations of geological conditions, ambient temperature and actual operation, then a specific control strategy should be adopted to keep the system operating stably by adjusting the operating parameters. In this work, for the off-design operation, the subcooling is fixed at 2 K for both ORCs, and the superheating is fixed at 5 K for subcritical ORC. A control strategy which maximizes the net power output is employed, and off-design performance analysis is carried out with variable geothermal water mass flow rate (m_{gw}), geothermal water inlet temperature (T_{gw}) and cooling water inlet temperature (T_{cw}).

To predict the off-design performance of a specified operation point, the values of m_{gw} , T_{gw} and T_{cw} should be given, the rotational speed of refrigerant pump (N_{RP}), turbine guide vane angle (α_{02}) and cooling water mass flow rate (m_{cw}) are regarded as control variables to adjust the system performance. The ORC system in this work is for power generation and supposed to connect to the grid, therefore the rotational speed of turbine remains constant. To conduct the submodel performance prediction, some operation parameters need to be previously assumed. For subcritical ORC, the assumed variables include turbine inlet pressure (P_1), condensation pressure (P_2). The turbine inlet temperature (T_1) can be obtained by the fixed superheating and P_1 . While for supercritical ORC, one more variable, namely T_1 should be assumed. For both subcritical and supercritical ORCs, according to the values of P_1 , P_2 , α_{02} and T_1 , the working fluid mass flow rate (m_{wf}), thermodynamic state at the outlet, as well as the off-design performance of the turbine can be determined by the turbine submodel. Then the off-design performances of condenser, refrigerant pump and evaporator (vapor generator) can be successively calculated by the corresponding submodels. It is noteworthy that the assumed operation parameters need to be adjusted until the calculated results agree with the actual component properties. In this work, optimizations based on genetic algorithm are respectively performed for subcritical and supercritical ORCs. The net power output is chosen as optimization objective, and the control variables mentioned above are regarded as decision variables. The detailed flow chart of off-design performance optimization is shown in Figure 7.

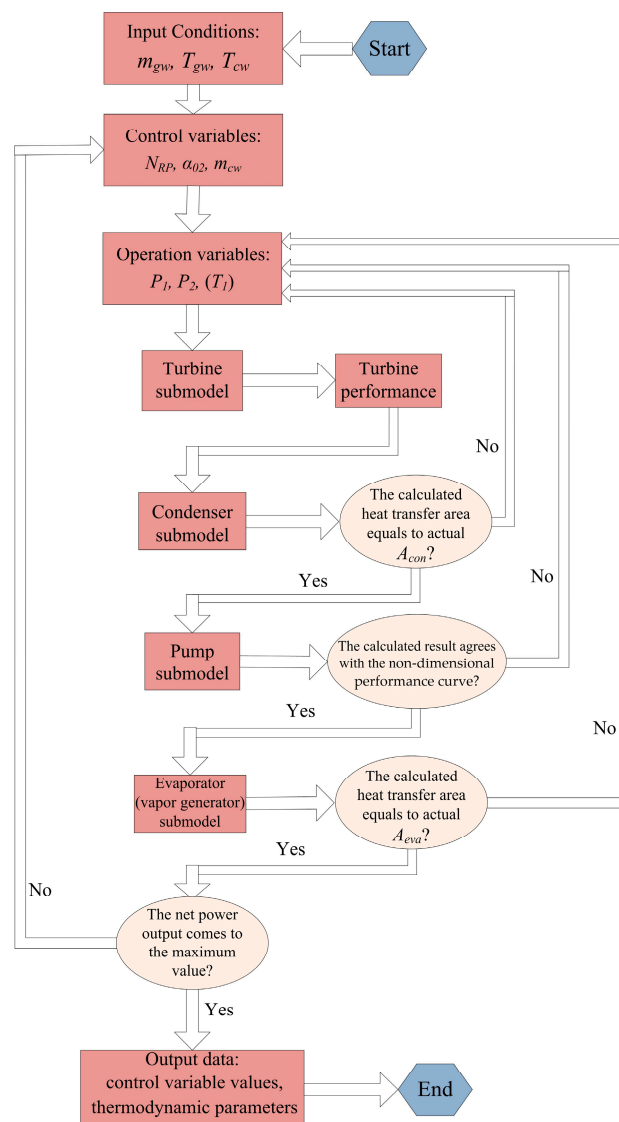


Figure 7. The detailed flow chart of off-design performance optimization.

4.2. Various Geothermal Water Mass Flow Rates

In this section, subcritical and supercritical ORCs with various m_{gw} are optimized, meanwhile T_{gw} and T_{cw} are fixed at the designed values. As displayed in Figure 8, the variations of the optimal control variables with m_{gw} are similar for subcritical and supercritical ORCs. As m_{gw} grows, α_{02} and N_{RP} both gradually increase. The growth of α_{02} is obvious, while the increase in N_{RP} is slight. In addition, m_{cw} first gradually increases and then becomes stable with m_{gw} for both ORCs, but the overall change is fairly small.

To further look into the off-design performances of ORCs with m_{gw} , the optimal operation parameters are also analyzed. For both ORCs, P_1 , namely the pressure of heater (evaporator or vapor generator), is roughly constant, and P_2 slowly rises with m_{gw} , as shown in Figure 9a,b. For supercritical ORC, T_1 nearly remains constant. The m_{wf} of the whole system is equivalent to the turbine mass flow rate. In this paper, supersonic flow always appears in the turbine nozzle due to the high expansion ratio, then the mass flow rate reaches the critical value. Thus, m_{wf} only depends on P_1 , T_1 and α_{02} .

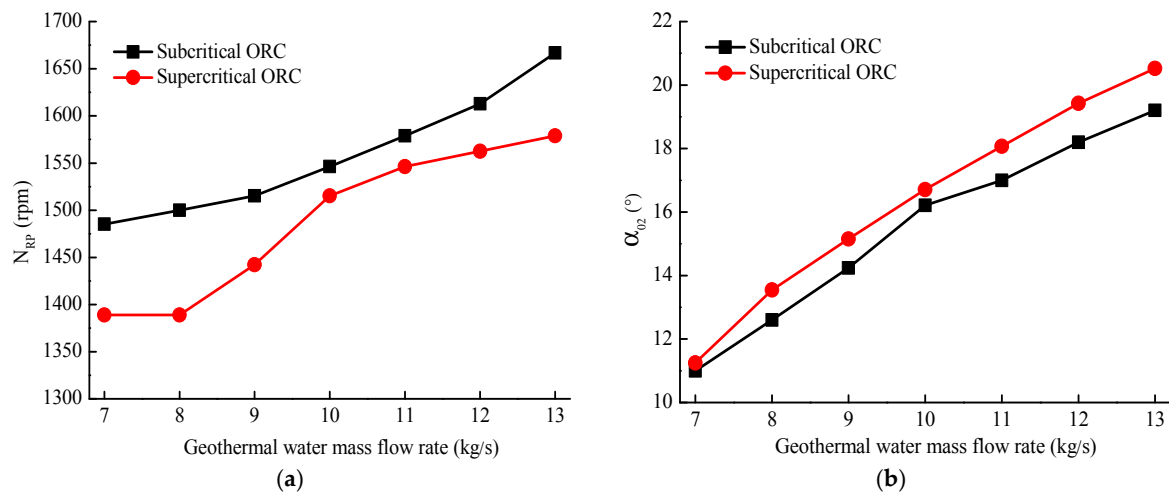


Figure 8. Variations of optimal control variables with geothermal water mass flow rate: (a) Turbine guide vane angle; (b) Refrigerant pump rotational speed.

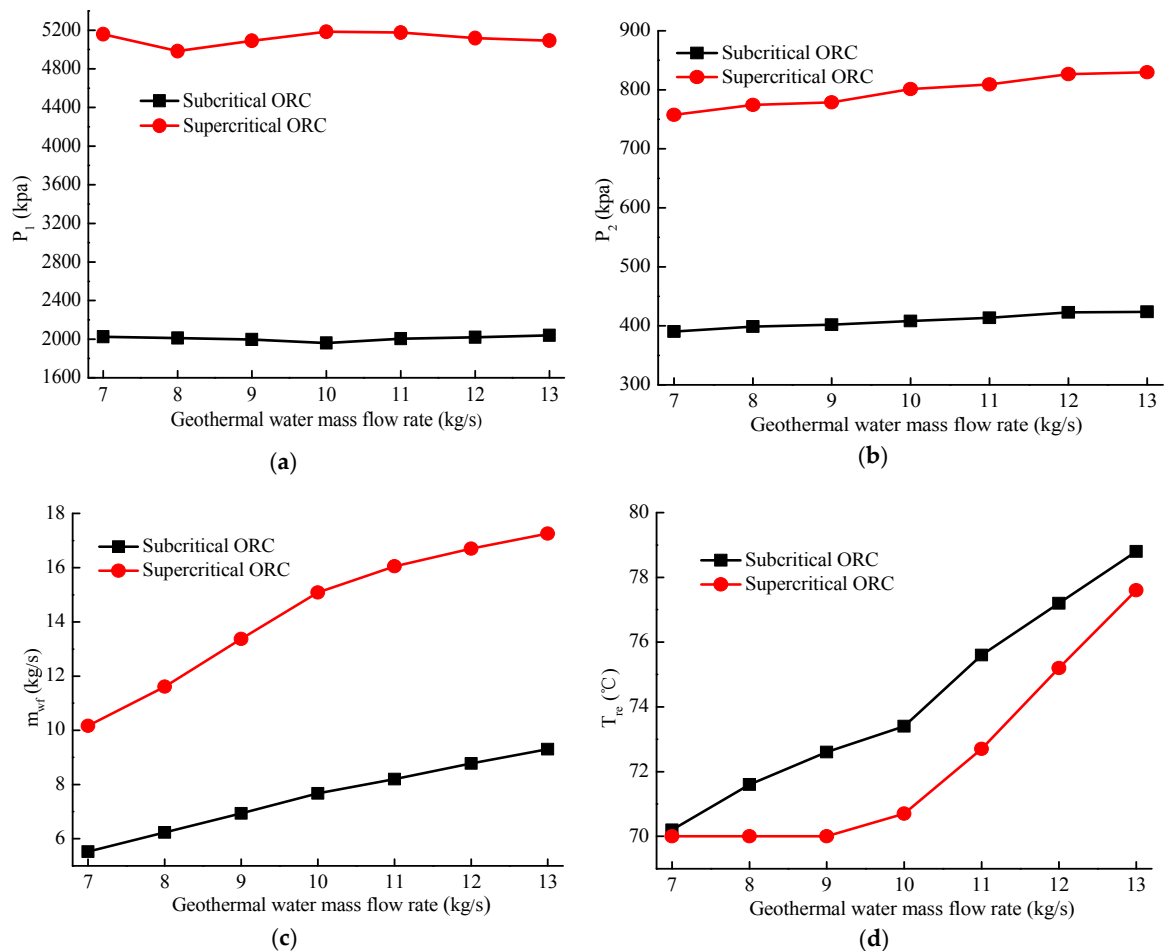


Figure 9. Variations of optimal operation parameters with geothermal water mass flow rate: (a) Turbine inlet pressure; (b) Condensation pressure; (c) Working fluid mass flow rate; (d) Geothermal water reinjection temperature.

As displayed in Figure 9c, for both ORCs, m_{wf} grows with m_{gfw} , which is mainly due to the increase in α_{O2} . The enthalpy rise in the evaporator (vapor generator) is stable due to the roughly constant T_1

and P_1 , and m_{wf} increases to absorb more heat from geothermal water. Meanwhile, the heat transfer rate in the condenser also grows, but m_{cw} changes very little. The slow increase in P_2 means the condensation temperature increases, then the condenser pinch temperature difference tends to be larger, which could satisfy the higher heat transfer rate in the condenser. As to the refrigerant pump, for both ORCs, with the increase in m_{gw} , the pump head is almost constant while the volumetric flow rate gradually grows due to the rising m_{wf} . Thus, a slow increase in N_{RP} simultaneously satisfies the pump head and volumetric flow rate (see Figure 8b).

The lower the geothermal water reinjection temperature (T_{re}), the more fully the geothermal energy is utilized. However, T_{re} should not be lower than 70 °C to avoid the silica oversaturation. As displayed in Figure 9d, for subcritical ORC, as m_{gw} grows, the utilization of geothermal energy drops, which can be deduced by the growing T_{re} . This may be due to the limited heat transfer area of the evaporator, while for supercritical ORC, when m_{gw} is smaller than the design value, T_{re} comes to the minimum allowed value of 70 °C, and m_{wf} degrades rapidly as m_{gw} falls (see Figure 9c). This can be explained by the fact that if m_{wf} does not decrease fast, the working fluid would absorb more heat from geothermal water, leading to the consequence that T_{re} is lower than 70 °C. When m_{gw} is greater than designed value, T_{re} grows rapidly with m_{gw} , which implies the heat amount absorbed by the working fluid becomes relatively small, resulting in a slow increase in m_{wf} .

For both ORCs, as m_{gw} grows, both the turbine power output and the power consumed by refrigerant pump rise owing to the increase in m_{wf} , and the power consumed by cooling water pump changes very little because of the small variation of m_{cw} . Since the increased turbine power output more than compensates for the increase in power consumed by the pumps, the net power output (P_{net}) rises with m_{gw} , as shown in Figure 10. Although P_{net} of supercritical ORC is always greater than that of subcritical ORC, the difference between them becomes smaller when m_{gw} deviates from the design value, and this is mostly due to the variation of turbine power output. For supercritical ORC, when m_{gw} is smaller than the design value, the m_{wf} degrades rapidly to satisfy the constraint of T_{re} , resulting in a quick decline in turbine power output, while when m_{gw} is greater than the design value, the slow growth of m_{wf} leads to a slow increase in turbine power output.

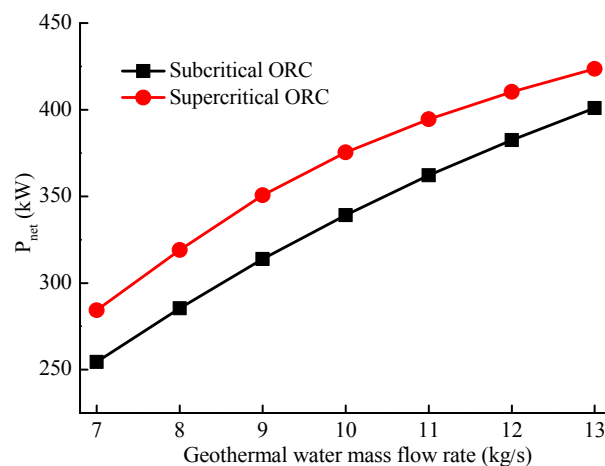


Figure 10. Variation of optimal net power output with geothermal water mass flow rate.

4.3. Various Geothermal Water Inlet Temperatures

In this part, subcritical and supercritical ORCs with various T_{gw} are optimized, meanwhile m_{gw} and T_{cw} are fixed at the designed values. The variations of optimal control variables are showed in Figure 11. For supercritical ORC, α_{02} basically remains the same value, while for subcritical ORC, a slightly decline can be observed. It is noteworthy that abnormal small α_{02} emerges when T_{gw} reaches the lowest value of 130 °C for both ORCs. Besides, for both ORCs, N_{RP} gradually increases with T_{gw} , and m_{cw} remains basically stable.

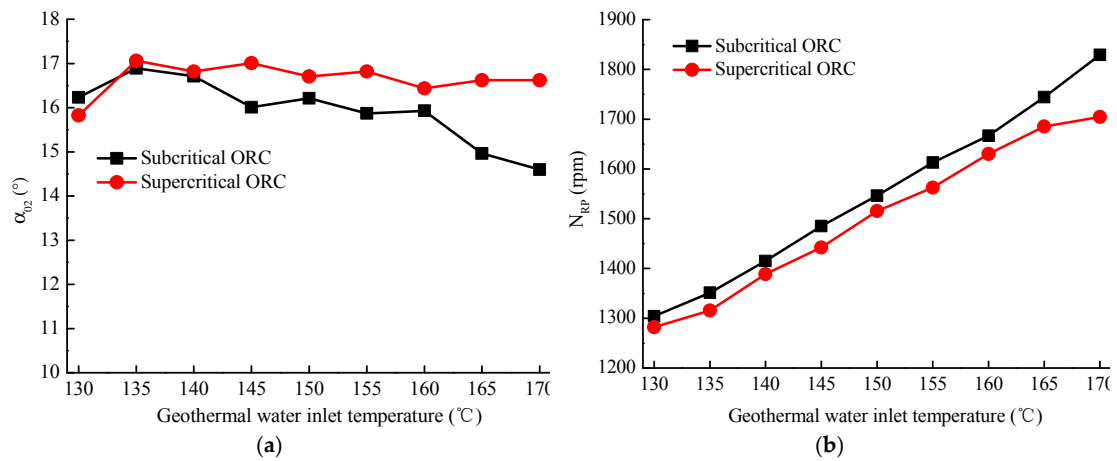


Figure 11. Variations of optimal control variables with geothermal water inlet temperature: (a) Turbine guide vane angle; (b) Refrigerant pump rotational speed.

The variations of optimal operation parameters with T_{gw} are shown in Figure 12. For both ORCs, P_1 gradually increases and P_2 slightly rises with T_{gw} , as shown in Figure 12a,b. For supercritical ORC, as T_{gw} grows, T_1 also gradually increases to generate a better temperature match between working fluid and geothermal water.

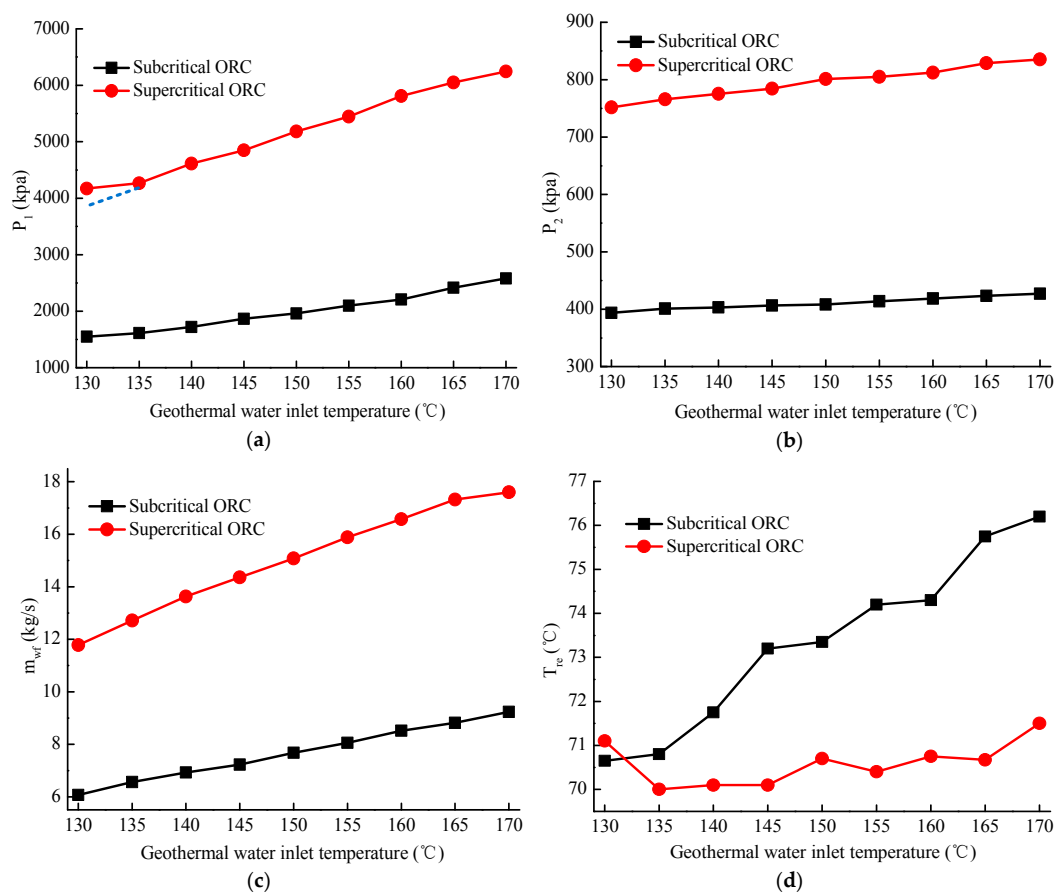


Figure 12. Variations of optimal operation parameters with geothermal water inlet temperature: (a) Turbine inlet pressure; (b) Condensation pressure; (c) Working fluid mass flow rate; (d) Geothermal water reinjection temperature.

As presented in Figure 12c, for both ORCs, m_{wf} gradually increases with T_{gw} . For supercritical ORC, α_{02} is nearly constant, the increase of m_{wf} is mainly determined by higher P_1 and T_1 . For subcritical ORC, although α_{02} basically decreases slowly, which means that m_{wf} has a decline trend, higher P_1 and T_1 can make up for this trend, consequently m_{wf} grows. As to the refrigerant pump, for both ORCs, N_{RP} adds with T_{gw} to satisfy the increases in volumetric flow rate and pump head, which are mainly caused by the increasing m_{wf} and difference between P_1 and P_2 , respectively.

As displayed in Figure 12d, for both ORCs, T_{re} generally increases as T_{gw} rises. Likewise, when T_{gw} comes to the minimum value of 130 °C, T_{re} becomes abnormal. For subcritical ORC, when T_{gw} changes from 135 °C to 130 °C, the decline rate of T_{re} slows down significantly, this may be due to the unusual small α_{02} (see Figure 11a), which leads to a small m_{wf} , then the restriction on the lowest T_{re} (70 °C) can be satisfied. For supercritical ORC, abnormal high T_{re} emerges when T_{gw} reaches 130 °C. This is because when T_{gw} reaches 130 °C, P_1 tends to be lower than the critical pressure of 4.06 Mpa for R134a (see the dashed line in Figure 12a). However, P_1 must be higher than the critical pressure to meet the supercritical condition, and high P_1 contributes to large m_{wf} , which leads to abnormal small α_{02} (see Figure 11a) to balance m_{wf} , eventually the geothermal energy fails to be fully utilized, and abnormal high T_{re} emerges.

For both ORCs, P_{net} gradually increases with T_{gw} , and P_{net} of supercritical ORC is greater than that of subcritical ORC, as displayed in Figure 13. As T_{gw} rises, working fluid per unit mass flow rate can produce more power due to the higher T_1 and P_1 , and m_{wf} also grows, thus turbine power output increases. The power consumed by refrigerant pump also grows owing to the increases of m_{wf} and difference between P_1 and P_2 . The power consumed by cooling water pump changes very little due to the small variation of m_{cw} . Eventually, P_{net} increases since the increased turbine power output can make up for the increase of power consumed by the pumps.

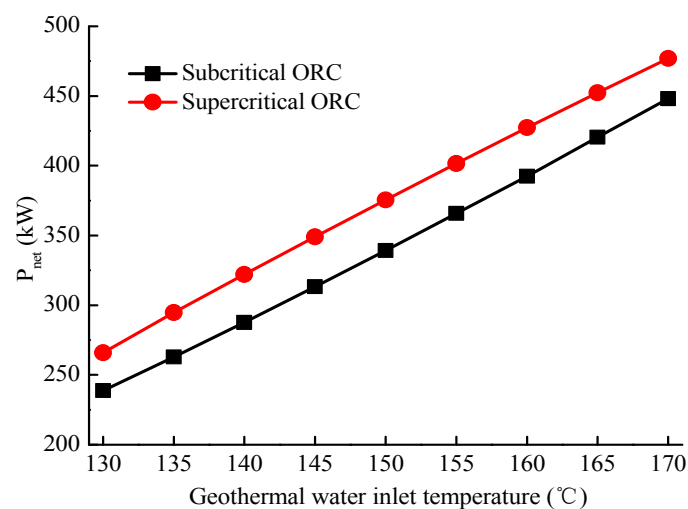


Figure 13. Variation of optimal net power output with geothermal water inlet temperature.

4.4. Various Cooling Water Inlet Temperatures

In this section, subcritical and supercritical ORCs with various T_{cw} are optimized, meanwhile m_{gw} and T_{gw} are fixed at the designed values. As shown in Figure 14a, for both ORCs, α_{02} first rises and then drops with T_{cw} , but the maximum α_{02} corresponds to different T_{cw} which is 25 °C for supercritical ORC and 15 °C for subcritical ORC. As presented in Figure 14b, N_{RP} is nearly constant for subcritical ORC, while N_{RP} first increases and then decreases with T_{cw} for supercritical ORC, and the maximum N_{RP} also corresponds to T_{cw} of 25 °C. Nonetheless, the variations of α_{02} and N_{RP} are overall small for both ORCs. In addition, m_{cw} is approximately steady for both ORCs.

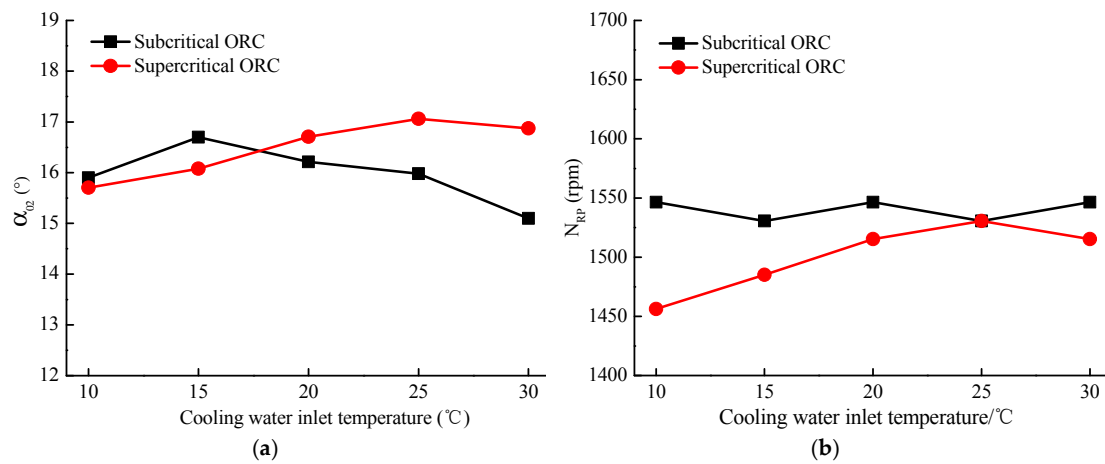


Figure 14. Variations of optimal control variables with cooling water inlet temperature: (a) Turbine guide vane angle; (b) Refrigerant pump rotational speed.

As presented in Figure 15a, as T_{cw} increases, for supercritical ORC, P_1 keeps roughly constant, while for subcritical ORC, P_1 slowly rises except the abnormal high P_1 which corresponds to T_{cw} of 10 °C. For both systems, P_2 gradually increases, as shown in Figure 15b.

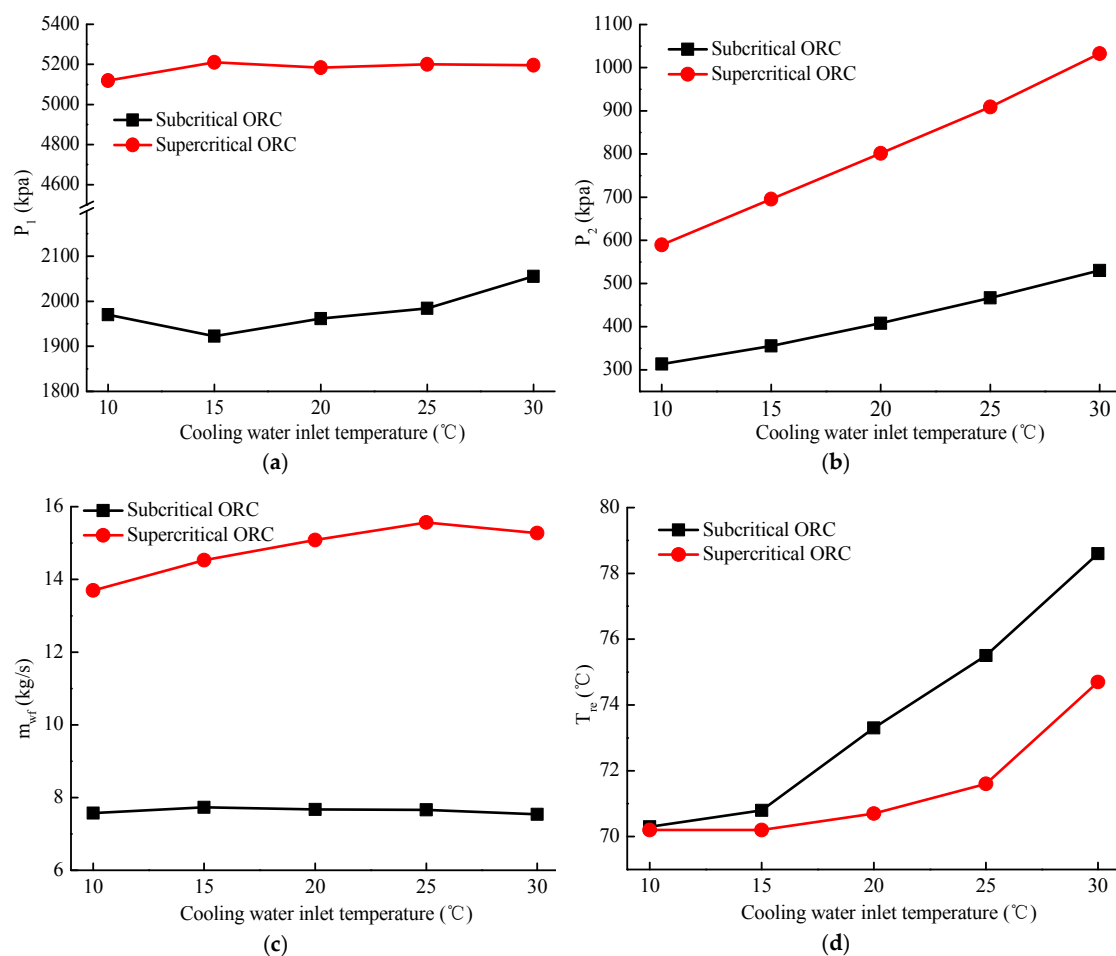


Figure 15. Variations of optimal operation parameters with cooling water inlet temperature: (a) Turbine inlet pressure; (b) Condensation pressure; (c) Working fluid mass flow rate; (d) Geothermal water reinjection temperature.

Figure 15c illustrates the variation of m_{wf} with T_{cw} . For supercritical ORC, owing to the slight variations of T_1 and P_1 , the variation of m_{wf} is similar with that of α_{02} . For subcritical ORC, m_{wf} is almost constant, this is mainly because the variations of P_1 and α_{02} are just opposite (see Figures 14a and 15a), and their effects on m_{wf} offset each other. As to the refrigerant pump, for both ORCs, the pump head is roughly constant as T_{cw} increases, N_{RP} mainly varies to satisfied the variation of volumetric flow rate, which is consistent with the change in m_{wf} . Thus, the variation of N_{RP} is just similar with that of m_{wf} for both ORCs. As displayed in Figure 15d, for both ORCs, T_{re} generally decreases as T_{cw} drops. This indicates that ORC with lower T_{cw} tends to utilize geothermal energy more fully, which is mainly determined by the lower P_2 . However, the decline rate of T_{re} is uneven because of the lowest T_{re} restriction of 70 °C. For supercritical ORC, when T_{cw} is lower than 25 °C, T_{re} is close to 70 °C, and the decline rate of T_{re} obviously slows down. In this case, the lowest T_{re} restriction is activated, α_{02} reduces as T_{cw} declines (see Figure 14a); meanwhile P_1 and T_1 are roughly constant, resulting in the decrease of m_{wf} , so that T_{re} is not lower than 70 °C. As to subcritical ORC, when T_{cw} is lower than 15 °C, the decline rate of T_{re} slows down, and the lowest T_{re} restriction is activated. Thus, P_1 and α_{02} become abnormal when T_{cw} reaches 10 °C (see Figures 14a and 15a). For both ORCs, as T_{cw} drops, the turbine power output grows owing to the decrease in P_2 , the power consumed by refrigerant pump is almost constant due to the small changes of m_{wf} and difference between P_1 and P_2 , and the power consumed by cooling water pump changes very little. Thus, P_{net} grows as T_{cw} drops, as shown in Figure 16. On the whole, P_{net} of subcritical ORC is always smaller than that of supercritical ORC, however, the difference between them presents a decrease trend as T_{cw} drops, which is owing to the reduction in m_{wf} of supercritical ORC.

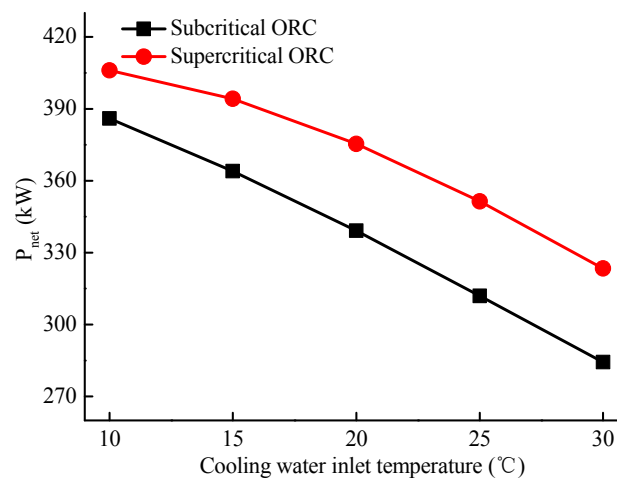


Figure 16. Variation of optimal net power output with cooling water inlet temperature.

4.5. Various Geothermal Water Inlet Temperatures and Cooling Water Inlet Temperatures

In practical operation of geothermal ORC power system, m_{gw} can be actively regulated to some extent, but T_{gw} influenced by geological condition and T_{cw} determined by ambient temperature depend on objective conditions. These two variables are independent of each other and can simultaneously change. Thus, the off-design performances of both ORCs are further discussed with various T_{gw} and T_{cw} .

Figure 17a shows that the variations of α_{02} are quite different for subcritical and supercritical ORC. For subcritical ORC, α_{02} first basically remains constant then drops with T_{gw} , while for supercritical ORC, α_{02} first increases then becomes roughly stable with T_{gw} . As displayed in Figure 17b, N_{RP} gradually grows with T_{gw} for both ORCs. As T_{cw} varies, N_{RP} is roughly constant for subcritical ORC, while for supercritical ORC, when T_{cw} is lower than 20 °C, N_{RP} has a declining trend as T_{cw} drops.

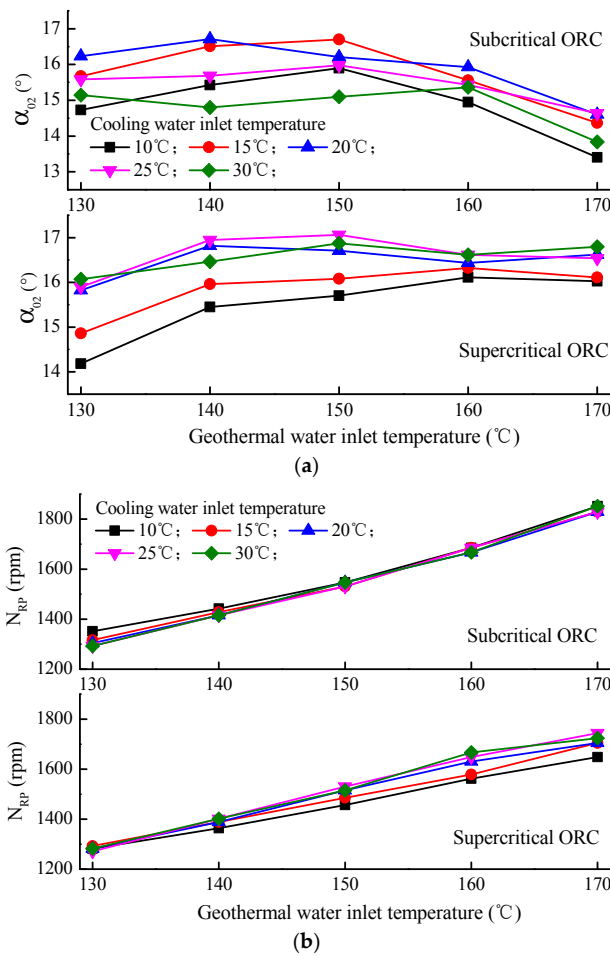


Figure 17. Variations of optimal control variables with geothermal water and cooling water inlet temperatures: (a) Turbine guide vane angle; (b) Refrigerant pump rotational speed.

Figure 18a,b illustrate that P_1 gradually increases and P_2 slowly rises with T_{gw} , while P_1 does not change significantly and P_2 gradually increases with T_{cw} , for both ORCs. As shown in Figure 18c, m_{wf} gradually grows with T_{gw} for both ORCs. As T_{cw} varies, m_{wf} is roughly constant for subcritical ORC, while for supercritical ORC, the variations of m_{wf} are similar with that of N_{RP} (see Figure 17b). When T_{cw} is low, the decline trend of m_{wf} ensures that T_{re} is not lower than 70 °C.

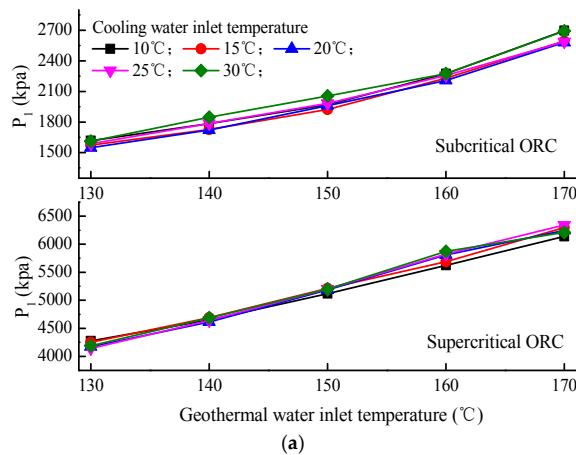


Figure 18. Cont.

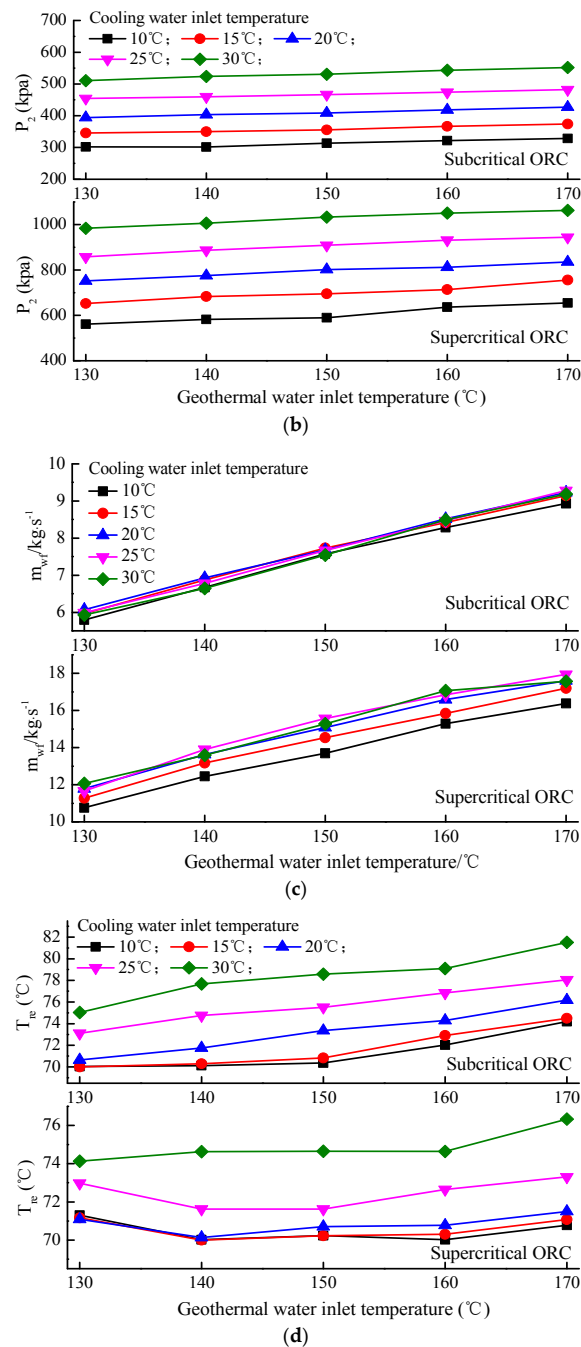


Figure 18. Variations of optimal operation parameters with geothermal water and cooling water inlet temperatures: (a) Turbine inlet pressure; (b) Condensation pressure; (c) Working fluid mass flow rate; (d) Geothermal water reinjection temperature.

Figure 18d illustrates that for both ORCs, lower T_{gw} and T_{cw} leads to lower T_{re} , and supercritical ORC is more likely to activate the constraint of T_{re} . This is mainly due to the varying temperature of the working fluid during the transition from liquid to vapor in the vapor generator, which leads to a better temperature match between working fluid and geothermal water. Notably, for supercritical ORC, when T_{gw} comes to 130 °C, abnormal high T_{re} appears, which may be owing to the supercritical condition restriction. As presented in Figure 19, for both ORCs, higher T_{gw} and lower T_{cw} bring about the increase in P_{net} . The P_{net} of supercritical ORC is always greater than that of subcritical ORC. However, for supercritical ORC, the growth rate of P_{net} slows down with the decrease of T_{cw} (below

20 °C), leading to smaller difference of P_{net} between supercritical and subcritical ORCs. This is mainly owing to the reduction of m_{wf} (see Figure 18c), which is caused by the constraint of T_{re} .

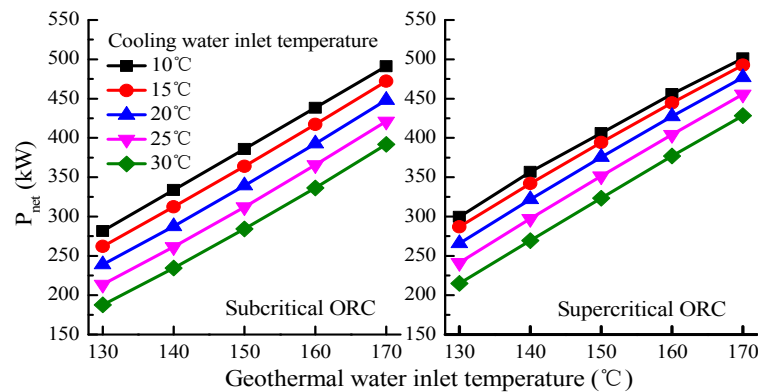


Figure 19. Variation of optimal net power output with geothermal water and cooling water inlet temperatures.

5. Conclusions

In this study, the parameter designs of subcritical and supercritical ORCs applied in geothermal power systems were firstly conducted under the design conditions. Then the off-design performance prediction model of ORC was established based on specially designed turbine and heat exchangers. Lastly, a specific optimal control strategy was proposed to maximum the net power output, and the off-design performances of subcritical and supercritical ORCs were comprehensively analyzed and compared under the optimal control strategy. The main conclusions of this work can be summarized as follows:

For both ORCs, under the optimal control strategy, greater geothermal water mass flow rate, higher geothermal water inlet temperature, lower cooling water inlet temperature bring about larger net power output. As geothermal water mass flow rate grows, the turbine guide vane angle gradually increases, and the refrigerant pump rotational speed slowly increases; the turbine inlet pressure changes very little, and the condensing pressure slowly rises. Owing to the increase in turbine guide vane angle, the working fluid mass flow rate rises to absorb more heat from geothermal water, leading to the growth in net power output. As the geothermal water inlet temperature increases, the turbine guide vane angle is relatively stable while the refrigerant pump rotational speed grows; the turbine inlet pressure gradually increases, the condensing pressure slowly rises, and the working fluid mass flow rate grows. The rise of net power output is mainly owing to the increases of turbine inlet pressure and working fluid mass flow rate. With cooling water inlet temperature drops, the turbine guide vane angle and the refrigerant pump rotational speed change a little; the turbine inlet pressure and the working fluid mass flow rate are roughly constant, while the condensing pressure significantly declines. The increase in net power output is mainly determined by the reduced condensing pressure.

Generally, under off-design operating conditions, the optimal control strategies of subcritical and supercritical ORCs are roughly approximate, and the variations of net power output of them are similar. The net power output of supercritical ORC is always greater than that of subcritical ORC, and the difference between them tends to drop when the supercritical ORC activates the restriction of geothermal water reinjection temperature. It is worth noting that smaller the geothermal water mass flow rate, the lower geothermal water inlet temperature and lower cooling water inlet temperature are inclined to activate the restriction of reinjection temperature, especially for supercritical ORC, which is due to the better temperature match in the vapor generator. When the restriction of reinjection temperature is activated, the turbine guide vane angle tends to decrease, resulting in a reduction in the working fluid mass flow rate to ensure that the reinjection temperature is not less than 70 °C, which further leads to a decreasing tendency of the net power output.

The proposed optimal control strategy can provide references and guidelines for the off-design operation regulation of subcritical and supercritical ORC systems. On the basis of this research, the next steps of our work are to establish a comprehensive dynamic model of ORC systems, study the dynamic characteristics under off-design conditions, and put forward a reasonable control logic and specific controller model.

Acknowledgments: This work is financially supported by the Innovative Research Team in University of Ministry of Education of China (IRT1280).

Author Contributions: All authors contributed to this work by collaboration. Changwei Liu completed the main parts of the research work. Tiyu Gao verified the work and actively contributed to finalizing the manuscript.

Conflicts of Interest: The authors declare no conflict of interest.

Nomenclature

A	area	[m ²]
Bd	Bond number	[-]
Bo	Boiling number	[-]
b	blade height	[mm]
c	absolute velocity	[m/s]
cd	channel distance	[mm]
c_p	constant pressure specific heat	[kJ/(kg-K)]
D	hydraulic diameter	[m]
g	gravitational acceleration	[m/s ²]
G	mass velocity	[kg/s]
h	enthalpy	[J/kg]
H	pump head	[m]
K	loss coefficient	[-]
L	loss	[J/kg]
M	loss model multiplier	[-]
m	mass flow rate	[kg/s]
N	rotational speed	[rpm]
n	incidence angle	[°]
P	power	[kW]
	pressure	[kPa]
Pl	plate length	[m]
Pr	Prandtl number	[-]
Pt	Plate thickness	[mm]
Pw	Plate width	[m]
Q	heat transfer rate	[kW]
q	heat flux	[W/m ²]
q	volumetric flow rate	[m ³ /s]
r	radius	[mm]
T	temperature	[°C]
U/C_0	velocity ratio	[-]
u	circular velocity	[m/s]
w	relative velocity	[m/s]
x	vapor quality;	[-]
Z	blade number	[-]
α	absolute fluid velocity angle	[°]
β	relative fluid velocity angle	[°]
γ	latent heat of vaporization	[J/kg]
δ	clearance	[m]
η	efficiency	[%]
θ	chevron angle	[°]

λ	thermal conductivity	[W/m-K]
μ	viscosity	[N-s/m ²]
ρ	density	[kg/m ³]

Subscripts

1–8	state points of ORCs
01–04	state points in turbine
b	bulk
cr	critical
cw	cooling water
de	design
df	disc friction
e	exit energy
eq	equivalent
g	gas
gw	geothermal water
i	incidence
in	inlet
l	liquid
m	mean
out	outlet
p	passage
RP	refrigerant pump
r	radial component
s	isentropic
u	tangential component
w	wall
wf	working fluid
WP	cooling water pump
st	stagnant

References

- Chen, H.; Goswami, D.Y.; Stefanakos, E.K. A review of thermodynamic cycles and working fluids for the conversion of low-grade heat. *Renew. Sustain. Energy Rev.* **2010**, *14*, 3059–3067. [[CrossRef](#)]
- Zhang, S.; Wang, H.; Tao, G.; Zhang, S.; Wang, H.; Tao, G. Performance comparison and parametric optimization of subcritical Organic Rankine Cycle (ORC) and transcritical power cycle system for low-temperature geothermal power generation. *Appl. Energy* **2011**, *88*, 2740–2754.
- Guo, C.; Du, X.; Goswami, D.Y.; Yang, L. Investigation on working fluids selection for organic rankine cycles with low-temperature heat sources. *Int. J. Green Energy* **2016**, *13*, 556–565. [[CrossRef](#)]
- Liu, C.; Gao, T.; Zhu, J.; Xu, J. Performance optimization and economic analysis of geothermal power generation by subcritical and supercritical Organic Rankine Cycles. In Proceedings of the ASME Turbo Expo 2016: Turbomachinery Technical Conference and Exposition, Seoul, Korea, 13–17 June 2016.
- Sauret, E.; Rowlands, A.S. Candidate radial-inflow turbines and high-density working fluids for geothermal power systems. *Energy* **2011**, *36*, 4460–4467. [[CrossRef](#)]
- Pan, L.; Wang, H. Improved analysis of Organic Rankine Cycle based on radial flow turbine. *Appl. Therm. Eng.* **2013**, *61*, 606–615. [[CrossRef](#)]
- Baines, N.C. A meanline prediction method for radial turbine efficiency. In Proceedings of the International 6th Conference on Turbocharging and Air Management Systems, London, UK, 3–5 November 1998; Volume 11, pp. 45–56.
- Li, Y.; Ren, X.D. Investigation of the organic Rankine cycle (ORC) system and the radial-inflow turbine design. *Appl. Therm. Eng.* **2016**, *96*, 547–554. [[CrossRef](#)]

9. Zheng, Y.; Hu, D.; Cao, Y.; Dai, Y. Preliminary design and off-design performance analysis of an Organic Rankine Cycle radial-inflow turbine based on mathematic method and CFD method. *Appl. Therm. Eng.* **2017**, *112*, 25–37. [[CrossRef](#)]
10. Wang, J.; Wang, M.; Li, M.; Xia, J.; Dai, Y. Multi-objective optimization design of condenser in an organic Rankine cycle for low grade waste heat recovery using evolutionary algorithm. *Int. Commun. Heat Mass Transf.* **2013**, *45*, 47–54. [[CrossRef](#)]
11. Calise, F.; Capuozzo, C.; Carotenuto, A.; Vanoli, L. Thermoeconomic analysis and off-design performance of an organic Rankine cycle powered by medium-temperature heat sources. *Sol. Energy* **2014**, *103*, 595–609. [[CrossRef](#)]
12. Song, J.; Gu, C.W.; Ren, X. Parametric design and off-design analysis of organic Rankine cycle (ORC) system. *Energy Convers. Manag.* **2016**, *112*, 157–165. [[CrossRef](#)]
13. Gabbriellini, R. A novel design approach for small scale low enthalpy binary geothermal power plants. *Energy Convers. Manag.* **2012**, *64*, 263–272. [[CrossRef](#)]
14. Fu, B.R.; Hsu, S.W.; Lee, Y.R.; Hsieh, J.C.; Chang, C.M.; Liu, C.H. Effect of off-design heat source temperature on heat transfer characteristics and system performance of a 250-kW organic Rankine cycle system. *Appl. Therm. Eng.* **2014**, *70*, 7–12. [[CrossRef](#)]
15. Fu, B.R.; Hsu, S.W.; Lee, Y.R.; Hsieh, J.C.; Chang, C.M.; Liu, C.H. Performance of a 250 kW organic Rankine cycle system for off-design heat source conditions. *Energies* **2014**, *7*, 3684–3694. [[CrossRef](#)]
16. Ibarra, M.; Rovira, A.; Alarcón-Padilla, D.C.; Blanco, J. Performance of a 5 kW e Organic Rankine Cycle at part-load operation. *Appl. Energy* **2014**, *120*, 147–158. [[CrossRef](#)]
17. Nusiaputra, Y.Y.; Wiemer, H.J.; Kuhn, D. Thermal-economic modularization of small, organic Rankine cycle power plants for mid-enthalpy geothermal fields. *Energies* **2014**, *7*, 4221–4240. [[CrossRef](#)]
18. Mazzi, N.; Rech, S.; Lazzaretto, A. Off-design dynamic model of a real Organic Rankine Cycle system fuelled by exhaust gases from industrial processes. *Energy* **2015**, *90*, 537–551.
19. Hu, D.; Li, S.; Zheng, Y.; Wang, J.; Dai, Y. Preliminary design and off-design performance analysis of an Organic Rankine Cycle for geothermal sources. *Energy Convers. Manag.* **2015**, *96*, 175–187. [[CrossRef](#)]
20. Hu, D.; Zheng, Y.; Wu, Y.; Li, S.; Dai, Y. Off-design performance comparison of an organic Rankine cycle under different control strategies. *Appl. Energy* **2015**, *156*, 268–279. [[CrossRef](#)]
21. Usman, M.; Imran, M.; Yang, Y.; Lee, D.H.; Park, B.S. Thermo-economic comparison of air-cooled and cooling tower based Organic Rankine Cycle (ORC) with R245fa and R1233zde as candidate working fluids for different geographical climate conditions. *Energy* **2017**, *123*, 353–366. [[CrossRef](#)]
22. Rajabloo, T.; Bonalumi, D.; Iora, P. Effect of a partial thermal decomposition of the working fluid on the performances of orc power plants. *Energy* **2017**, *133*, 1013–1026. [[CrossRef](#)]
23. Liu, L.; Zhu, T.; Ma, J. Working fluid charge oriented off-design modeling of a small scale Organic Rankine Cycle system. *Energy Convers. Manag.* **2017**, *148*, 944–953. [[CrossRef](#)]
24. Liu, Q.; Duan, Y.; Yang, Z. Performance analyses of geothermal organic Rankine cycles with selected hydrocarbon working fluids. *Energy* **2013**, *63*, 123–132. [[CrossRef](#)]
25. Toffolo, A.; Lazzaretto, A.; Manente, G.; Paci, M. A multi-criteria approach for the optimal selection of working fluid and design parameters in Organic Rankine Cycle systems. *Appl. Energy* **2014**, *121*, 219–232. [[CrossRef](#)]
26. Lecompte, S.; Huisseune, H.; Broek, M.V.D.; Schampheleire, S.D.; Paepe, M.D. Part load based thermo-economic optimization of the Organic Rankine Cycle (ORC) applied to a combined heat and power (CHP) system. *Appl. Energy* **2013**, *111*, 871–881. [[CrossRef](#)]
27. Ge, Z.; Wang, H.; Wang, H.T.; Wang, J.J.; Li, M.; Wu, F.Z.; Zhang, S.Y. Main parameters optimization of regenerative organic Rankine cycle driven by low-temperature flue gas waste heat. *Energy* **2015**, *93*, 1886–1895. [[CrossRef](#)]
28. Feidt, M.; Kheiri, A.; Pelloux-Prayer, S. Performance optimization of low-temperature power generation by supercritical ORCs (organic Rankine cycles) using low GWP (global warming potential) working fluids. *Energy* **2014**, *67*, 513–526.
29. Vetter, C.; Wiemer, H.J.; Kuhn, D. Comparison of sub- and supercritical Organic Rankine Cycles for power generation from low-temperature/low-enthalpy geothermal wells, considering specific net power output and efficiency. *Appl. Therm. Eng.* **2013**, *51*, 871–879. [[CrossRef](#)]

30. Lecompte, S.; Huisseune, H.; Broek, M.V.D.; Vanslambrouck, B.; Paepe, M.D. Review of organic Rankine cycle (ORC) architectures for waste heat recovery. *Renew. Sustain. Energy Rev.* **2015**, *47*, 448–461. [[CrossRef](#)]
31. Marcuccilli, F.; Zouaghi, S. Radial inflow turbines for kalina and organic Rankine cycles. In Proceedings of the European Geothermal Congress 2007, Unterhaching, Germany, 30 May–1 June 2007.
32. Wasserbauer, C.A.; Glassman, A.J. *Fortran Program for Predicting Off-Design Performance of Radial-Inflow Turbines*; National Aeronautics and Space Administration: Washington, DC, USA, 1975.
33. Meitner, P.L.; Glassman, A.J. *Computer Code for Off-Design Performance Analysis of Radial-Inflow Turbines with Rotor Blade Sweep*; NASA Lewis Research Center: Cleveland, OH, USA, 1983.
34. Ventura, C.A.M.; Jacobs, P.A.; Rowlands, A.S.; Petrie-Repar, P.; Sauret, E. Preliminary design and performance estimation of radial inflow turbines: An automated approach. *J. Fluids Eng.* **2012**, *134*. [[CrossRef](#)]
35. Forooghi, P.; Hooman, K. Experimental analysis of heat transfer of supercritical fluids in plate heat exchangers. *Int. J. Heat Mass Transf.* **2014**, *74*, 448–459. [[CrossRef](#)]
36. Klemeš, J.J. *Compact Heat Exchangers for Energy Transfer Intensification: Low Grade Heat and Fouling Mitigation*; CRC Press: Boca Raton, FL, USA, 2015.
37. Bejan, A.; Kraus, A.D. *Heat Transfer Handbook*; John Wiley & Sons: Hoboken, NJ, USA, 2003.
38. García-Cascales, J.; Vera-García, F.; Corberán-Salvador, J.; González-Maciá, J. Assessment of boiling and condensation heat transfer correlations in the modelling of plate heat exchangers. *Int. J. Refrig.* **2007**, *30*, 1029–1041. [[CrossRef](#)]
39. Amalfi, R.L.; Vakili-Farahani, F.; Thome, J.R. Flow boiling and frictional pressure gradients in plate heat exchangers. Part 2: Comparison of literature methods to database and new prediction methods. *Int. J. Refrig.* **2016**, *61*, 185–203. [[CrossRef](#)]
40. Yan, Y.Y.; Lio, H.C.; Lin, T.F. Condensation heat transfer and pressure drop of refrigerant r-134a in a plate heat exchanger. *Int. J. Heat Mass Transf.* **1999**, *42*, 993–1006. [[CrossRef](#)]



© 2017 by the authors. Licensee MDPI, Basel, Switzerland. This article is an open access article distributed under the terms and conditions of the Creative Commons Attribution (CC BY) license (<http://creativecommons.org/licenses/by/4.0/>).